

**A Novel Few-Cycle Optical Source in the
Mid-Infrared**

by
Peter Ra Krogen

B.S., University of California Santa Barbara (2012)

Submitted to the Department of Electrical Engineering and Computer
Science

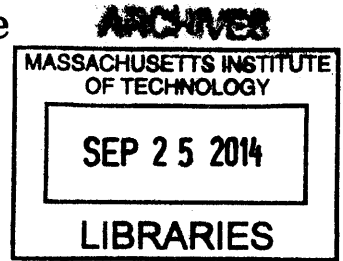
in partial fulfillment of the requirements for the degree of
Masters of Science in Electrical Engineering and Computer Science

at the

MASSACHUSETTS INSTITUTE OF TECHNOLOGY

September 2014

© Massachusetts Institute of Technology 2014. All rights reserved.



Author **Signature redacted**
Department of Electrical Engineering and Computer Science
August 29, 2014

Certified by **Signature redacted**
Franz X. Käertner
Adjunct Professor
Thesis Supervisor

Certified by **Signature redacted**
Erich P. Ippen
Elihu Thomson Professor of Electrical Engineering Professor of Physics
Emeritus
Thesis Supervisor

Accepted by **Signature redacted**
Leslie A. Kolodziejski
Chair of the Committee Graduat Students

A Novel Few-Cycle Optical Source in the Mid-Infrared

by

Peter Ra Krogen

Submitted to the Department of Electrical Engineering and Computer Science
on August 29, 2014, in partial fulfillment of the
requirements for the degree of
Masters of Science in Electrical Engineering and Computer Science

Abstract

In this thesis, I designed, simulated, and implemented a novel optical pulse generation system which is shown to be able to generate exceptionally short optical pulses in the mid-infrared, tunable from $2\text{-}4\mu\text{m}$ with pulse widths as low as 1.5 optical cycles at $3.5\mu\text{m}$ (18fs). Energies as high as $1\mu\text{J}$ were achieved, representing a peak power of roughly 100MW, at a 1kHz repetition rate, with excellent beam quality. The system was based on adiabatic difference frequency generation in an aperiodically polled lithium niobate crystal of an amplified, mode-locked Ti:Sapphire laser system.

Thesis Supervisor: Franz X. Kaertner
Title: Adjunct Professor

Thesis Supervisor: Erich P. Ippen
Title: Elihu Thomson Professor of Electrical Engineering Professor of Physics Emeritus

Acknowledgments

I would like to acknowledge all of those who have helped me along the long journey that has lead me to where I am now. First and foremost, I would like to thank my advisors Professor Franz Kaertner and Erich Ippen, who have provided me an opportunity to pursue my dreams in laser development, and my mentor Jeff Moses who has been an invaluable source of skills, guidance, and support. Furthermore, I give my most heartfelt gratitude to my parents who encouraged me to pursue my interests in electrical engineering, and supporting me through the decades of schooling needed to make this all possible. I also must thank all of those who have been involved in construction of the various laser components used in this system, in particular Shu-Wei Huang, and Haim Suchowski—it would have been impossible to achieve the results presented here without the years of work put in by my predecessors.

I also give special thanks to my professors at UCSB and MIT, in particular Associate Professor Luke Theogarajin; without his guidance I surely would not have ended up at MIT. Additionally, I must send my gratitude to the student chapter of IEEE at UCSB, and all of their members, who provided a space to hone my engineering skills by working on projects in a fun and relaxed environment.

Finally, I give my most heartfelt thanks to my girlfriend Melissa Johnson, who has always been everything I could ask for.

THIS PAGE INTENTIONALLY LEFT BLANK

Contents

1	Introduction	11
1.1	Motivation	13
1.2	Adiabatic Difference Frequency Generation	14
2	Simulation	21
2.1	Introduction	21
2.2	Analytical	21
2.3	Quasi-Monochromatic	23
2.4	Pulse Propagation	25
3	Experiments	31
3.1	Introduction	31
3.2	Implementation	31
3.3	Depletion Measurements	33
3.4	Generation of Uncompressed Continuum	35
3.5	Spectral Amplitude Transfer	37
3.6	Spectral Phase Transfer	38
4	Conclusions	41

THIS PAGE INTENTIONALLY LEFT BLANK

List of Figures

1-1	Other Few-Cycle MIR Sources	12
1-2	Block Sphere[26]	16
1-3	Conversion Efficiency for Constant $\Delta k(z)$	18
1-4	Conversion Efficiency for Adiabatically Varied $\Delta k(z)$	18
2-1	Conversion Phase for Varied $\Delta k(z)$	23
2-2	Quasi-Monochromatic Simulation	24
2-3	Pulse Propagation Simulation	27
2-4	Simulated - Compressed Pulse	28
2-5	Simulation - Alternate Compressor	29
2-6	Simulation - No Compressor	30
3-1	Pulse Synthesizer Overview [13]	32
3-2	ADFG Experimental Setup [25]	33
3-3	NIR Depletion [13]	34
3-4	Uncompressed MIR Spectrum	35
3-5	MIR Beam Profile	36
3-6	Spectral Amplitude Transfer [13]	37
3-7	4-cycle Tunable MIR Source	39
3-8	Pulse Compressed to Sub-2-Cycle Duration	40

THIS PAGE INTENTIONALLY LEFT BLANK

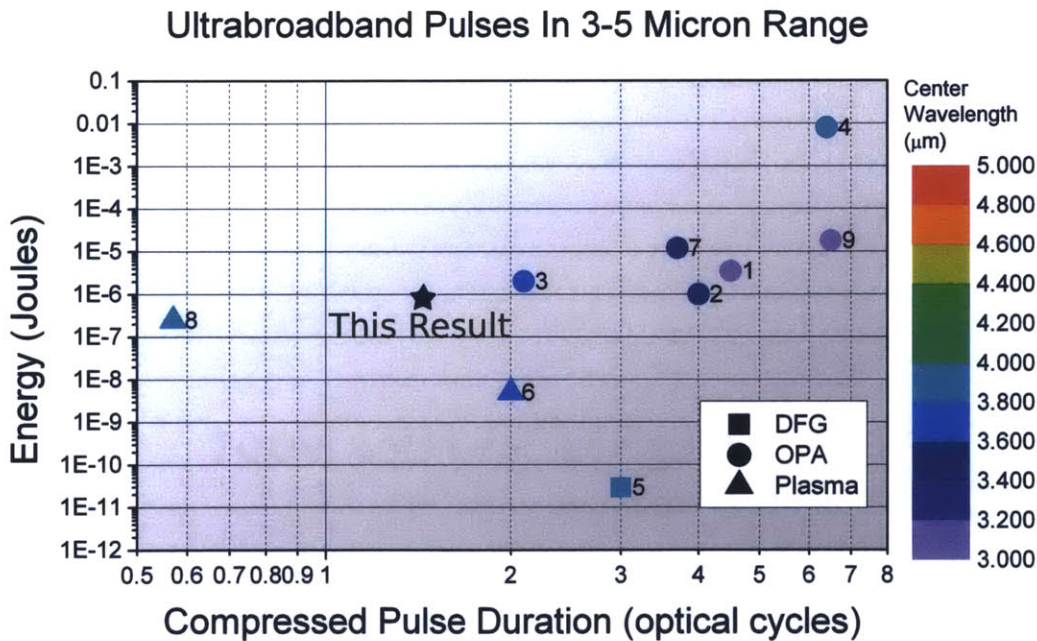
Chapter 1

Introduction

Terahertz through the mid-IR (MIR, defined here as 2-5 μm) has always been a 'dark' region for coherent sources, with groups pushing from both the lower frequency side through faster transistors and diodes, to roughly 300 μm (1THz) [28] and from the higher frequency side with 'optical' devices such as quantum cascade lasers, and lasers combined with nonlinear processes, such as difference frequency generation (DFG), etc). However these sources are generally limited in power and/or prohibitively complicated/expensive. Of course, there are many applications which would benefit from better coherent sources, and as a result there is much active development in generating better mid-IR sources.

Of particular importance to the community are ultrafast pulsed sources, which offer both high peak powers (necessary for investigating nonlinear properties of materials) and broad bandwidths (which allow them to be used for spectroscopic applications). Such sources are typically constructed by converting pulses from a mode-locked near-infrared laser to the MIR through some nonlinear process, however it is also possible to directly generate the pulses, for example using a mode-locked quantum cascade laser [7]. Unfortunately, many of the existing techniques for generating ultrafast (a few optical cycles), broadband (bandwidth covering a significant fraction of an octave), energetic (μJ to mJ energies) mid-IR pulses, such as those required for driving high harmonic generation, performing nonlinear pump-probe spectroscopy, or any other strong-field laser-matter interaction in the MIR, are cumbersome and lim-

ited in performance. As a result there has been much activity in the field to improve the state of the art, and a wide variety of techniques are currently being pursued to generate such pulses, such as the use of carefully designed optical parametric oscillators (OPOs), plasma generation driven by near-IR (NIR defined here as 0.7-2 μm) [23], as well as difference frequency generation (DFG) or Optical Parametric Amplification (OPA). A brief summary of the current published results is given in Figure 1-1, which gives a summary of selected sources based on a variety of generation techniques. From this it can be seen that OPA techniques have been used to generate very high energies (many mJ of energy per pulse, tens of gigawatt peak powers), and plasma based techniques have been able to generate extremely short (sub-optical cycle), while this result represents a middle ground of short duration and high energy.



Summary of other MIR few-cycle sources, plotted against their energy and measured pulse duration 1 [9] 2 [3] 3 [6] 4 [1] 5 [24] 6 [21] 7 [15] 8 [20] 9 [10]

Figure 1-1: Other Few-Cycle MIR Sources

1.1 Motivation

There were 2 primary motivations for this project—the first was to take advantage of recent advancements in technology to create a more capable MIR source, and the second was to create a seed source required for experiments within the Kaertner group. The latter placed very stringent requirements on the source—it needed to fit well with the technology currently in use for the system (based on chirped pulse amplification of a broadband Ti:Sapphire seed laser, described in detail in [12]), and it needed to be able to produce pulses which are very broadband (ideally octave spanning), compressed (no temporal or spatial chirp), energetic (μJ level energies), and carrier envelope phase (CEP) stable, so that they could be amplified and then used for two-color spectroscopy experiments. A number of possible approaches were considered, but ultimately it was concluded that using difference frequency generation between a broadband NIR source (such as the Ti:Sapphire laser used in our laser system[12]) and narrowband pump source at $1\mu\text{m}$ (such as the Nd:YLF regenerative amplifier in our laser system[12]) to generate an idler in the MIR, which theoretically could span from $1.8\mu\text{m}$ into the THz region. This approach has the advantage that the properties of the NIR pulse are transferred to the MIR—a property which is extremely desirable for this application, because NIR sources with the necessary properties (μJ energies, controlled chirp, CEP stable, good spatial properties, etc) can be built with existing technology, and furthermore there already exists a source in our laser system system[12] which could easily be modified to work for this application (described in Section 3.2). This greatly simplifies the overall architecture, because most of the experimental work can be done on the NIR laser system, taking advantage of the wealth of technology which already exists for NIR laser sources, and then the pulses can be converted to the MIR at the end of the optical system and directly used for experiments. Unfortunately, as of several years ago, there was no crystal available which was capable of converting the full bandwidth needed with good efficiency, however there was a promising new technology being developed which offered a way to avoid this limitation—adiabatic difference frequency generation[26].

1.2 Adiabatic Difference Frequency Generation

Adiabatic difference frequency generation (ADFG) is a special case of three wave mixing (TWM) in a nonlinear medium with a second order susceptibility (that is to say, a material which is non-symmetric such that the polarization generated from an incident electric field contains a component proportional to the incident field squared)—for which the general theory was first described succinctly by Armstrong et al [2], shortly after the first demonstration of the laser in the early 1960's [14]. For the general case of TWM, one first considers 3 incident electric fields, to be called E_1 , E_2 , and E_3 , with center frequencies ω_1 , ω_2 , and ω_3 respectively, which satisfy the constraint that $\omega_1 + \omega_2 = \omega_3$, which are each represented as complex valued phasors. While propagating through the medium, these three fields interact through the nonlinearity in the medium, which allows energy to transfer among the 3 fields, as described by Equations 1.1-1.4, which can be easily derived from Maxwell's Equations by making the slowly varying envelope approximation[2].

$$\frac{\partial E_1}{\partial z} = -i \frac{\omega_1 d_{eff}}{n_1 c} E_2' E_3 e^{-i\Delta k z} \quad (1.1)$$

$$\frac{\partial E_2}{\partial z} = -i \frac{\omega_2 d_{eff}}{n_2 c} E_1' E_3 e^{-i\Delta k z} \quad (1.2)$$

$$\frac{\partial E_3}{\partial z} = -i \frac{\omega_3 d_{eff}}{n_3 c} E_1 E_2 e^{i\Delta k z} \quad (1.3)$$

$$\Delta k = k_3 - k_2 - k_1 \quad (1.4)$$

Where n_1 , n_2 , and n_3 , are the indices of refraction of the material at each center frequency, c is the speed of light in a vacuum, d_{eff} is the effective magnitude of the second order susceptibility, Δk the phase mismatch (which is a function of wavelength due to the material dispersion), and z is the propagation length through the material. In the general case (considering only linear dispersion of the material) the solution to 1.1-1.4 is a Jacobi Elliptic Integral. However in the case of a strong, undepleted E_2 , these expressions can be reduced to a simpler pair of coupled ordinary differential equations as shown below:

$$-i \frac{\partial A_1}{\partial z} = \kappa A_3 e^{-i\Delta k z} \quad (1.5)$$

$$-i \frac{\partial A_3}{\partial z} = \kappa' A_1 e^{i\Delta k z} \quad (1.6)$$

$$A_3 = \frac{E_3}{\sqrt{\kappa}}, A_1 = \frac{E_1}{\sqrt{\kappa'}} \quad (1.7)$$

$$\kappa = \frac{4\pi\omega_1\omega_2 d_{eff}}{\sqrt{n_1 n_3} c} E_2 \quad (1.8)$$

which, by no coincidence, possess a SU(2) symmetry and are the same as those that describe a nuclear magnetic resonance or the interaction of an electric field with a 2-level atom[4].

$$-i \frac{\partial C_g}{\partial z} = \Omega_0 C_n e^{-i\Delta t} \quad (1.9)$$

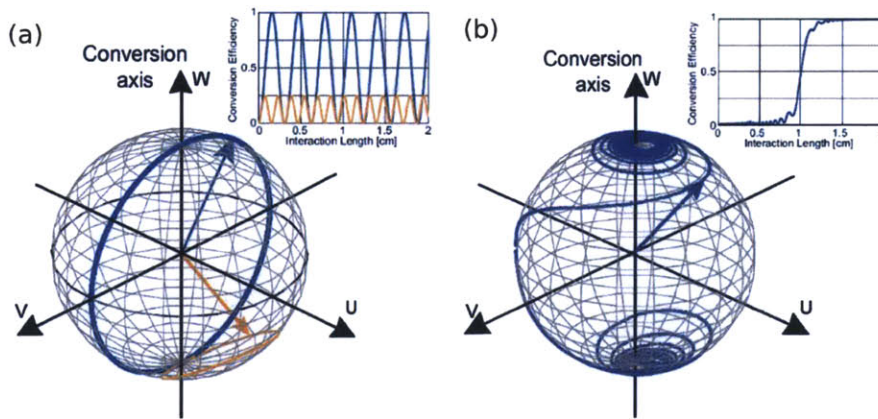
$$-i \frac{\partial C_n}{\partial z} = \Omega_0' C_g e^{i\Delta t} \quad (1.10)$$

This relation was noticed by Suchowski et al[26], who realized that with an undepleted E_2 wave it is possible, and straightforward even, to make a nonlinear optical system which contains a property analogous to rapid adiabatic passage, and that such a system would be able to greatly expand the phase matching bandwidth of existing nonlinear processes[26]. The phase mismatch Δk is represented by the frequency detuning between the energy of the applied electric field ($\hbar\omega$) and energy level of the absorption (the difference of the ground/excited states $C_n - C_g$), and the oscillation frequency Ω is related to the the effective nonlinear coefficient in the crystal, d_{eff} , applied intensity of the 'pump' field E_2 , the frequencies of the applied fields, etc.

This is convenient, because it means that the wealth of theory which has been developed to find creative ways to transfer between quantum states can be applied to find new ways of satisfying the phase matching condition in a nonlinear optical process[26]. In particular, in the case where one can vary the phase mismatch $\Delta k(z)$ with propagation (in this case this is achieved by varying the polling period in a

quasi-phase-matched structure, described in detail in Section 3.2) it is possible to drastically change the dynamics of the DFG process.

An intuitive way to describe this is to make use of the so called 'Bloch sphere', shown in Figure 1-2, which can be used to represent the transition between 2 quantum states, or in this case between 2 wavelengths of light. The formalism is straightforward in this case, the solutions to Equations 1.6-1.9 are visualized as planes intersecting a sphere, generating a circular trajectory. The south pole ($w = 0$) of the sphere represents the initial state (all photons at ω_3 , in the NIR, no conversion) and the north pole ($w = 1$) represents the final state (all photons at ω_1 , in the MIR, 100% conversion). Propagation through the nonlinear medium is represented by trajectories on the surface of the sphere, and the projection of any point on the sphere to the w axis directly gives the conversion efficiency.



Conversion efficiency plotted for a crystal with constant phase matching conditions (a) and with adiabatically varied phase matching conditions (b)

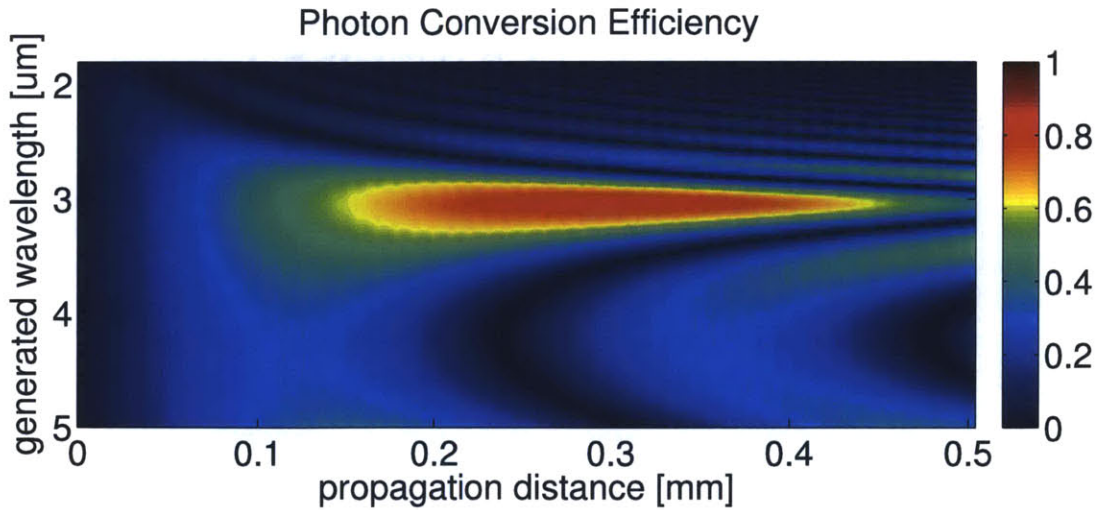
Figure 1-2: Bloch Sphere[26]

To generate a trajectory on the sphere, one draws a vector from the center to the initial state (ie, the south pole, or all photons at ω_3 , and then rotates about an angle related to the phase mismatch Δk , generating a circle which represents conversion and back-conversion cycles. Two typical trajectories are shown in Figure 1-2a, drawn in orange and blue, and their projection to the w axis is include in the inset. The blue trajectory shows perfect phase matching, and shows that if the system starts

at the south pole (all photons at ω_3) the conversion efficiency will go to unity (the north pole, all photons at ω_1) and then cycle back down to 0 again ad infinitum, as one would expect for the case of perfect phase matching with an undepleted pump ω_2 . The orange trajectory represents imperfect phase matching, and has the same general behavior as blue trajectory, however instead of going through the north pole it is at an angle, and its projection on the w axis never goes above 0.25. Also note, the oscillation period is higher than that of the perfect phase matching case, going through 2 cycles for conversion/back-conversion for every 1 cycle of the perfect phase matching case.

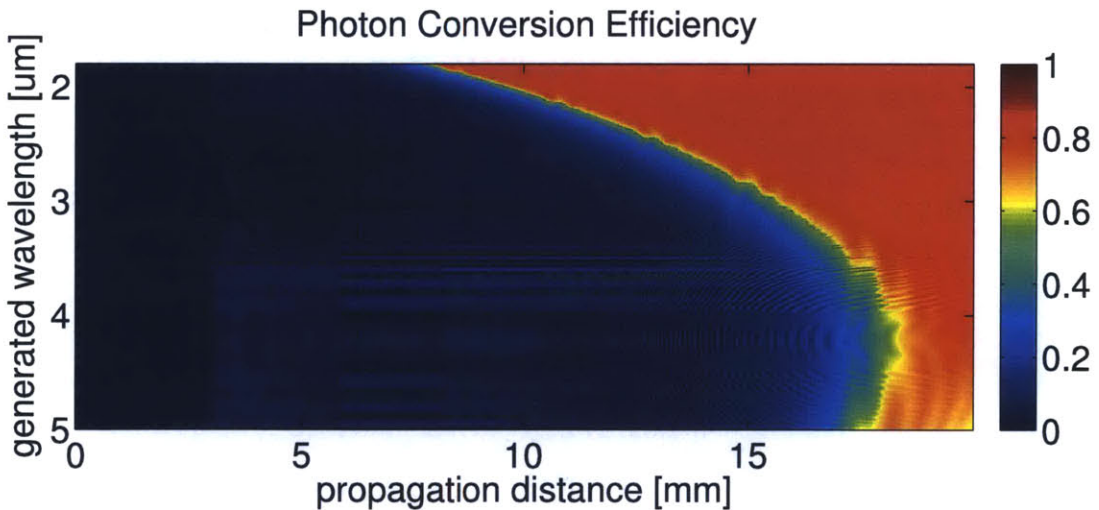
This exactly represents the problem faced for generating broadband MIR pulses using DFG—when the effects of dispersion are taken into account, it is not possible to get broadband conversion due to phase matching limitations. If one chooses the phase matching condition to be matched for 830nm→4000nm, then the blue trajectory will represent conversion to 4000nm, and the orange trajectory will roughly represent 800nm→3400nm. It is clear that good conversion can be had for the 830nm→4000nm case (100%), and mediocre conversion can be had for the 800nm→3400nm case (25%), *however* it not possible to satisfy both of these conditions at any point in the crystal because the conversion cycles have different periods for different phase mismatches. This can clearly be seen in Figure 1-3 which shows conversion efficiency for a LiNbO₃ crystal phase matched for 830nm→4000nm, which was generated using the simulation discussed in Chapter 2.4.

However, if one carefully varies the phase mismatch over the length of the nonlinear medium, the situation changes significantly, as can be seen in Figure 1-2b where the trajectories are no longer limited to circles about a fixed point, and in fact with a carefully chosen $\Delta k(z)$ it is possible to generate a trajectory such as that shown in Figure 1-2b, which is fundamentally different from those shown in Figure 1-2a, most notably because there is essentially no back conversion, such as can be seen in Figure 1-4 (note that the crystal length is 20mm in this case, instead of 0.5mm as in the constant case). Furthermore, this process is quite robust, however there are a few constraints placed on the optical system:



Generated using the pulse propagation simulation described in 2.4, under the same conditions as used to generate Figure 1-4, which were chosen to be similar to those used in the experiment. Pump intensity $12\text{GW}/\text{cm}^2$, seed intensity $1\text{MW}/\text{cm}^2$, using a flattop seed spectral profile chirped to approximately 10ps duration. Note the much shorter crystal length as compared to figure 1-4.

Figure 1-3: Conversion Efficiency for Constant $\Delta k(z)$



Generated using the pulse propagation simulation described in 2.4, under the same conditions as used to generate Figure 1-3, which were chosen to be similar to those used in the experiment. Pump intensity $12\text{GW}/\text{cm}^2$, seed intensity $1\text{MW}/\text{cm}^2$, using a flattop seed spectral profile chirped to approximately 10ps duration.

Figure 1-4: Conversion Efficiency for Adiabatically Varied $\Delta k(z)$

1. The middle wave E_2 should remain undepleted throughout the interaction
2. The middle wave E_2 should be narrowband (typically $<1\text{nm}$ of bandwidth)
3. The pulses should be chirped sufficiently that there is not significant temporal walkoff between the different waves
4. The rate at which the phase matching conditions change should be slow

This last constraint, that the rate at which the phase matching conditions vary must be slow, can be further constrained by the Landau-Zener result[29], which gives that the conversion efficiency (in this case, from E_3 to E_1) will asymptotically approach unity as the nonlinear coupling κ is increased, which, as defined in Equation 1.8, is a function of the material properties and the intensity of the pump E_2 , which gives rise to the following constraint:

$$\left| \frac{\delta \Delta k}{\delta z} \right| \ll \frac{(\Delta k^2 + \kappa^2)^{3/2}}{\kappa} \quad (1.11)$$

which puts a limit on how quickly the $\Delta k(z)$ can vary to get good conversion, or alternatively the minimum pump intensity for a given crystal geometry, a result which is experimentally verified[19], and discussed in detail in Section 3.3.

Furthermore, this situation is inherently broadband, due to the fact that $\Delta k(z)$ varies over the length of the nonlinear medium. By choosing a sufficiently large variation in $\Delta k(z)$ it is possible to phase match an arbitrarily large range of wavelengths (limited only by practical concerns, such as the ability to fabricate a crystal with the required polling period, material transparency, etc), *and* get nearly unity conversion at all phase matched wavelengths. Furthermore, this has been experimentally verified[25], where a periodically polled lithium niobate crystal was used to generate an octave-spanning idler spanning $2\text{-}5\mu\text{m}$ with greater than 85 percent conversion efficiency. This is discussed in detail in Section 3.4.

THIS PAGE INTENTIONALLY LEFT BLANK

Chapter 2

Simulation

2.1 Introduction

In order to develop a practical frequency conversion device, a variety of simulation tools were needed in order to evaluate different crystal designs. Fortunately, the crystals used for this project were designed by our collaborator Haim Suchowski [25] and fabricated by HC Photonics (HsinChu City, Taiwan), so the efforts at MIT could focus on the evaluation of different crystal designs and construction of a suitable experimental apparatus to produce the desired tunable and single-cycle pulses. Three primary simulation approaches were used, simple analytical calculations—discussed in Section 2.2, quasi-monochromatic numerical simulations—discussed in Section 2.3, and time dependent pulse propagation simulations—discussed in Section 2.4.

2.2 Analytical

The first calculations done for this project were based on the theory presented in [27], which allowed one to calculate the required pump intensity for a given crystal design (in particular, given the polling period as a function of propagation length and material properties of the crystal) based on Landau-Zener theory. This can be summarized neatly in a simple expression for the photon conversion efficiency from the NIR to MIR, Γ , in terms of the crystal design and pump intensity:

$$\Gamma = 1 - e^{-\pi \left| \frac{d\kappa^2}{dz} \right|} \quad (2.1)$$

$$\kappa^2 = \frac{2.232 d_{eff}^2 I_2}{n_1 n_2 n_3 \lambda_1 \lambda_3 c} \quad (2.2)$$

Where d_{eff} is the effective second-order susceptibility in pm/V , I_2 is the pump intensity in MW/cm^2 , n_1 , n_2 , n_3 , are signal, pump, and idler indices of refraction; λ_1 and λ_3 are signal and idler wavelengths in cm ; c is the speed of light in cm/s ; and the sweep rate $\frac{d\Delta k}{dz}$ is in cm^{-2} .

Furthermore, for the purposes of re-compressing the generated MIR idler to transform limited duration, it was of critical importance that accurate methods were available to calculate the dispersion experienced by the NIR/MIR pulses as they propagate through the crystal. Conveniently, the phase imparted by the actual conversion process is a constant value across all wavelengths (predicted by [26], and later confirmed in simulation in Section 2.4 and experimentally in Chapter 3.6), so it can be ignored when evaluating the dispersion—so long as the adiabaticity conditions are satisfied. However, there is a significant amount of material dispersion in the $LiNbO_3$ crystal used for this project, which must be taken into account. This is further complicated by the fact there is a significant difference between the dispersion at NIR and MIR wavelengths, so there is a significant 'effective' conversion phase introduced by the fact that each color in the NIR is transferred to the MIR at a different longitudinal location point in the crystal, as shown in Figure 2-1, so each color experiences a different ratio of dispersion evaluated at NIR and MIR wavelengths. This can be modeled quite simply by simply calculating the phase for each wavelength as a sum of phase due to linear propagation through the crystal, traveling a fraction of the length in the NIR and the remaining length in the MIR, and assuming the conversion happens instantly at the point at which the phase mismatch Δk is swept through 0 (perfect phase matching).

$$\psi(\omega) = k(\omega_{NIR}) * L_{NIR} + k(\omega_{MIR}) * L_{MIR} \quad (2.3)$$

The dispersion can then be evaluated by taking successive derivatives of $\psi(\omega)$ for each wavelength. Note - this can be calculated analytically given the material properties and crystal design, however due to the fact that L_{NIR} contains the polling period and the index of refraction, which must be calculated from Sellmeier coefficients, the analytical expression for the dispersion in this situation is quite messy. Regardless, it is easy to calculate either using computer aided symbolic math, or using numerical methods, and this provides an easy way to get an accurate estimate on the dispersion imparted on the pulse through propagation through the crystal.

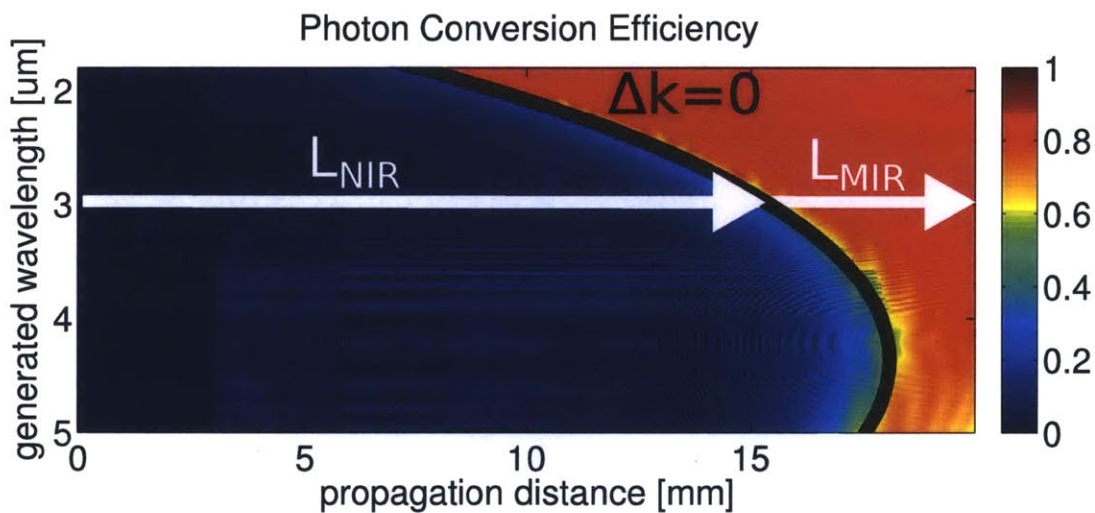


Figure 2-1: Conversion Phase for Varied $\Delta k(z)$

2.3 Quasi-Monochromatic

While it is possible to calculate most of the key parameters associated with these devices analytically, one must turn to numerical simulation to consider the real devices and parasitic effects associated with them, such as the effect of pump depletion, using a finite crystal length, the discrete polling period sizes, higher order dispersion, etc. For this we turned to a quasi-monochromatic simulation, which takes advantage of the fact that for this project the signal/idler pulses are strongly chirped, and there is relatively little coupling between any two wavelengths (for a given field). As a result,

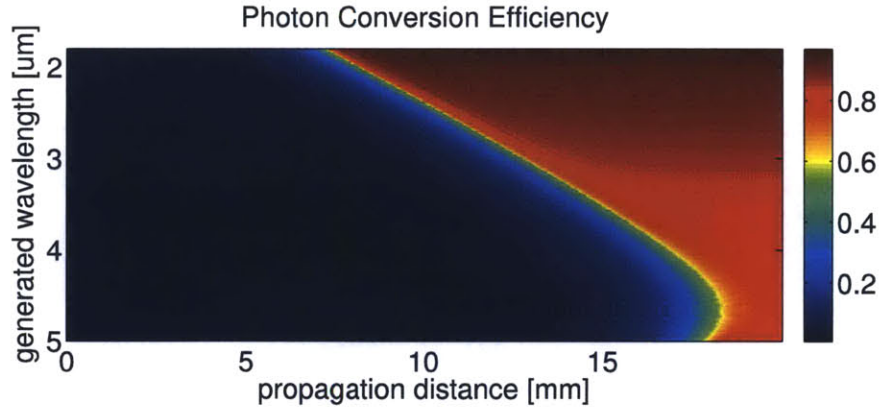


Figure 2-2: Quasi-Monochromatic Simulation

one can consider the conversion process for a monochromatic case, and ignore the time dependence of the conversion process. This greatly simplifies the calculations, as one can simply solve Equations 1.1-1.4 directly through numerical integration. A simple MATLAB script was used to do exactly this. It used a 4th-order Runge-Kutta solver to integrate Equations 1.1-1.4 for each wavelength of interest, and simple support code used for plotting, etc.

The results of a typical simulation are shown in Figure 2-2, which shows the conversion efficiency as a function of input wavelength and crystal longitudinal position, for the same crystal design used in the pulse simulations and experimental work, which clearly shows the broadband nature of the ADFG process. Furthermore, an estimate of the spectral phase could be extracted from the results of this simulation and was confirmed to be smooth and free of ripples which might cause problems recompressing the generated pulse. These initial results were promising, and encouraging enough that we decided to continue with the project and have the crystal fabricated. Note, due to the nature of this simulation, it cannot account for any of the effects due to the pulse nature of the process, such as temporal walkoff, temporal variations in the pump intensity, the effects of dispersion on the conversion process, etc.

2.4 Pulse Propagation

Due to the fact that a quasi-monochromatic simulation does not consider the pulse nature of this experiment, ultimately a more advanced simulation was needed to simulate the full ADFG conversion process. This led to the development of a simple pulse propagation simulation which uses the split-step method to solve the 1-D case of Maxwell's Equations, in a material which has an arbitrary dispersion (ie, non-instantaneous response), and a second-order susceptibility, under the slowly varying envelope approximation. Conveniently, a 1-D simulation was sufficient to model most of the interesting effects, due to collinear nature of the conversion, the lack of spatial walkoff in the process (Type-0 phase matching is used, with all waves propagating along the extraordinary axis of the crystal), and weak dependence of the conversion process on the intensity.

As the name implies, the simulation works by splitting the pulse propagation into 2 steps: a linear step which includes the effect of linear propagation through the material, and a nonlinear step which considers the nonlinearity in the material while ignoring the presence of the material dispersion which was accounted for in the linear step. Due to the nature of these 2 effects, it is much simpler to consider the effect of linear propagation in the frequency domain, and the effect of the nonlinearity in the time domain, so a Fourier transform is used to transform between to the frequency domain and back to the time domain at each step in the simulation. The exact expressions evaluated are:

Time Domain:

$$\frac{\partial E_1}{\partial z} = -i \frac{\omega_1 d_{eff}}{n_1 c} E_2' E_3 \quad (2.4)$$

$$\frac{\partial E_2}{\partial z} = -i \frac{\omega_2 d_{eff}}{n_2 c} E_1' E_3 \quad (2.5)$$

$$\frac{\partial E_3}{\partial z} = -i \frac{\omega_3 d_{eff}}{n_3 c} E_1 E_2 \quad (2.6)$$

Note: these are identical to the general case presented in expressions 1.1-1.4 with the phase mismatch Δk set to 0. As in the quasi-monochromatic case, these are

solved using a 4th-order Runge-Kutta integration.

Frequency Domain:

$$e_1(z + \Delta z) = e_1(z)e^{-ik_1(w)\Delta z} e^{\frac{iw\Delta z}{V_{frame}}} \quad (2.7)$$

$$e_2(z + \Delta z) = e_2(z)e^{-ik_2(w)\Delta z} e^{\frac{iw\Delta z}{V_{frame}}} \quad (2.8)$$

$$e_3(z + \Delta z) = e_3(z)e^{-ik_3(w)\Delta z} e^{\frac{iw\Delta z}{V_{frame}}} \quad (2.9)$$

Note: a retarded frame is used for the propagation, such that the pulse is shifted in time/space to keep it centered within the bounds of the simulation during its propagation. For this simulation the velocity of the retarded frame V_{frame} was selected to be the group velocity of the pump.

Finally, the relationship between the fields is a simple Fourier transform

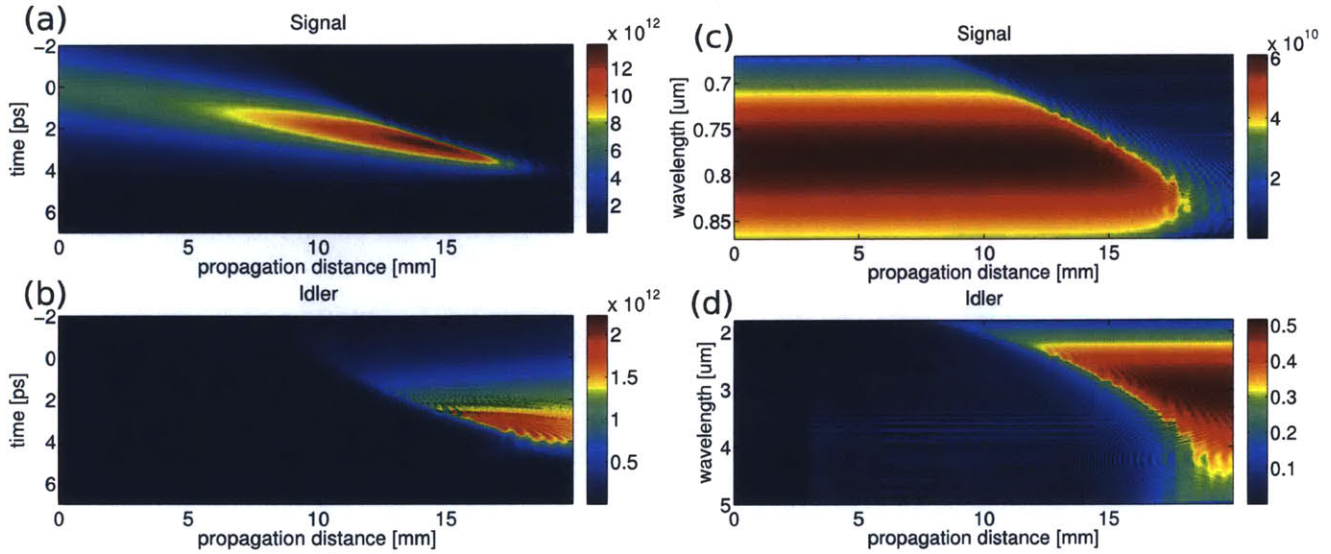
$$E_1 = \mathcal{F}(e_1) \quad (2.10)$$

$$E_2 = \mathcal{F}(e_2) \quad (2.11)$$

$$E_3 = \mathcal{F}(e_3) \quad (2.12)$$

Furthermore, a significant amount of support code was written to evaluate the results of this simulation, including functions to evaluate the dispersion imparted by propagation through the crystal, functions to model other dispersive elements in the system (stretcher, compressor, etc), functions to plot, save and recall data, etc. Note, due to the parallel nature of these equations, it is trivial to parallelize this simulation, and in fact using the `gpuArray()` command in MATLAB it was possible to convert the entire propagation simulation to run on a GPU. This allows for a complete 1-D simulation of the crystal used in this project to complete in approximately 15 minutes when running on commodity computer hardware (Intel core i7 quad core processor @ 4.0GHz, and an Nvidia GTX580 GPU).

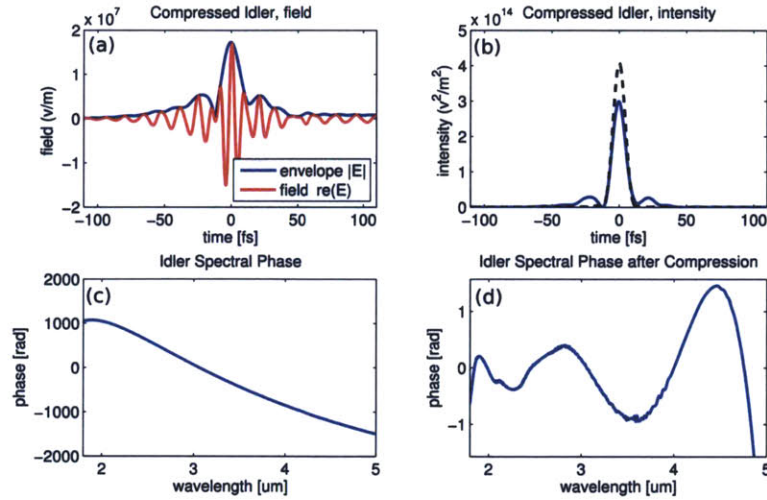
The results of this simulation turned out to be quite interesting, and allowed a number of potential pitfalls to be avoided in designing the experimental setup. Shown in Figure 2-3 is the frequency/time domain propagation of the NIR/MIR pulses as



Electric field (a,b in V/m) and Spectrum (c,d in W/Hz) as a function of crystal length, for the NIR (a,c) and MIR (b,d) fields, showing the adiabatic difference frequency generation.

Figure 2-3: Pulse Propagation Simulation

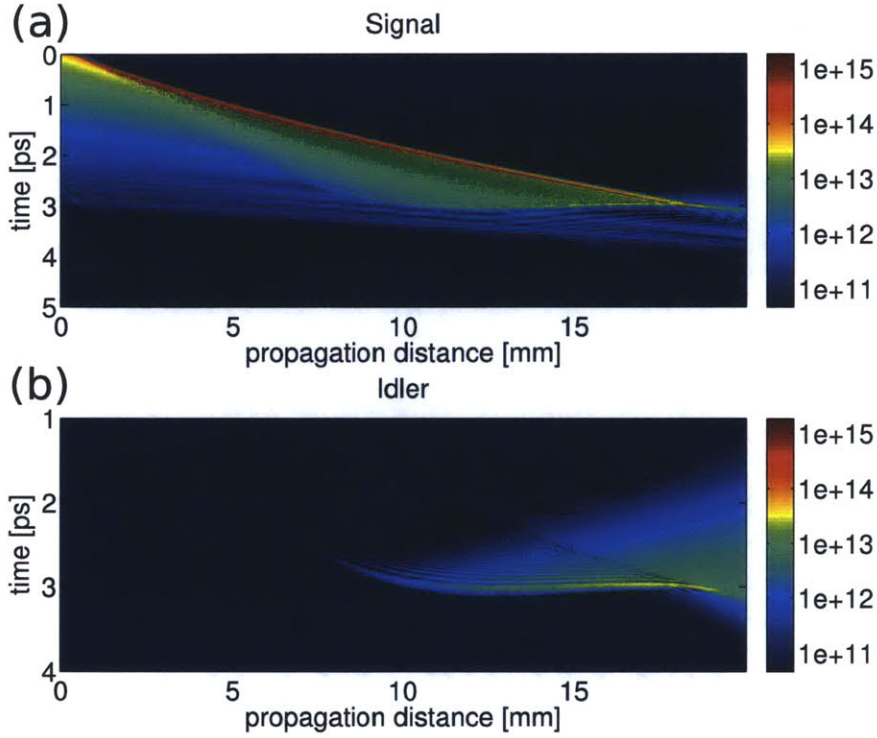
used in the experimental setup, which shows a nice cleanly chirped pulse throughout the propagation and good conversion of the NIR to the MIR. For this simulation, the pump pulse duration was $12ps$ FWHM (Fourier limited), the pump intensity was $12GW/cm^2$, the pump wavelength was $1.047\mu m$, the signal duration was $5ps$ FWHM (highly chirped), with an intensity of $1MW/cm^2$, which was chosen to be sufficiently small that the pump remains nearly undepleted. The signal was pre-chirped to compensate the dispersion of the ADFG crystal and compressor (which consisted of $20mm$ of bulk silicon) by applying a polynomial phase up to 4th-order (as could be applied using an acousto-optic programmable dispersive filter), such that after propagation through the compressor the signal was compressed to within 5% of its Fourier limit of $10fs$ (1.0 optical cycles), as shown in Figure 2-4. Additionally, the residual spectral phase is plotted both before and after the compressor, showing that there is some residual higher-order spectral phase on the pulse, which serves to add small wings on the pulse, as shown in Figure 2-4a, however these do not significantly reduce the peak intensity of the pulse and are of sufficiently low intensity that they will not affect most strong-field processes.



Compressed idler field (a), compressed idler intensity (b, solid) Fourier limited idler intensity (b,dashed), spectral phase after propagation through crystal (c), and residual phase after compression (d)

Figure 2-4: Simulated - Compressed Pulse

Additionally, Figure 2-5 shows a case where the compressor was made shorter, 5mm instead of 20mm , and the pre-chirp was adjusted to compensate, but the simulation conditions are otherwise held constant. This required a pre-chirp on the NIR pulse which was not ideal, which causes the pulse to be torn apart by 3rd/4th order dispersion in the crystal, resulting in a messy temporal profile. This does not appreciably affect the overall conversion process for weak signal pulses, however the peak intensity of the signal is significantly higher for this case (the peak electric field is nearly 100 times higher than that for the 20mm compressor shown in figure 2-3), so at higher seed intensities the pulses may be prone to parasitic nonlinear effects, which would make recompression impractical. This result demonstrates a potential pitfall associated with adiabatic frequency conversion, which comes from that fact the crystal lengths are quite long, so one must be mindful of the material dispersion and carefully select chirps throughout the system as to avoid generating compressed pulses in the crystal. However, this effect can also be quite beneficial. For example, in the crystal design used for this experiment (which is discussed in detail in [25]) the effective chirp imparted on the pulse as it is converted from the NIR to the MIR

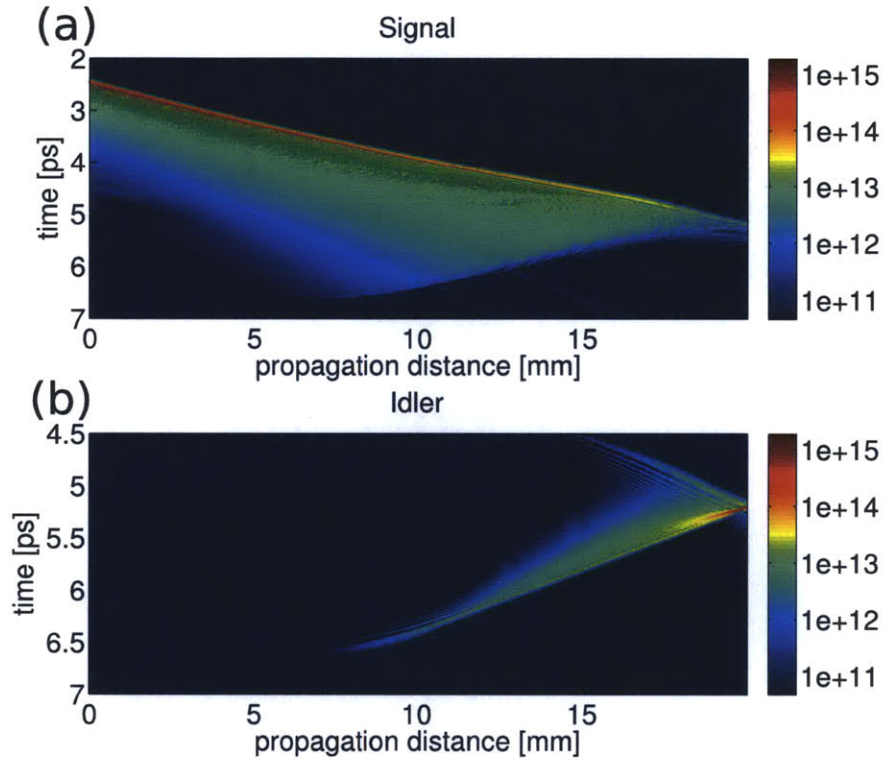


Electric field (a,b in V/m, note the log scale) as a function of crystal length, for the NIR (a) and MIR (b) fields, showing partial self compression of the NIR signal, followed by adiabatic difference frequency generation.

Figure 2-5: Simulation - Alternate Compressor

(which, as discussed in Section 2.2, is due primarily to the linear material dispersion and the fact that each wavelength is converted at a different longitudinal position in the crystal) is approximately $+700fs^2$ of group velocity dispersion, and $-22,000fs^3$ of third order dispersion. This is quite convenient for the purpose of chirped pulse frequency conversion, because most materials have positive third order dispersion, as do many stretcher designs. For example, in this experiment the combination of gratings+dazzler intrinsic dispersion represents approximately $-10,000fs^2$ of group velocity dispersion and $+32,000fs^3$ of third order dispersion, while the compressor represents approximately $+10,000fs^2$ of group velocity dispersion and $+15,000fs^2$ of third order dispersion, so the the effective chirp serves to partially compensate the higher order dispersion in the system which reduces the demands placed on the dispersion management scheme.

Finally, plotted in Figure 2-6 is the case where no compressor is used, and the pulse is pre-chirped such that the MIR idler is compressed in the ADFG crystal, with negligible chirp remaining as it exits the crystal. No changes were made to the simulation conditions as compared to Figure 2-3 or 2-5, other than changing the applied pre-chirp. This case is not ideal in terms of power handling, due to the fact that the idler is compressed to single cycle duration in the ADFG crystal, however it could be useful if high energies are not required.



Electric field (a,b in V/m, note the log scale) as a function of crystal length, for the NIR (a) and MIR (b) fields, showing the adiabatic difference frequency generation and compression of the idler.

Figure 2-6: Simulation - No Compressor

Chapter 3

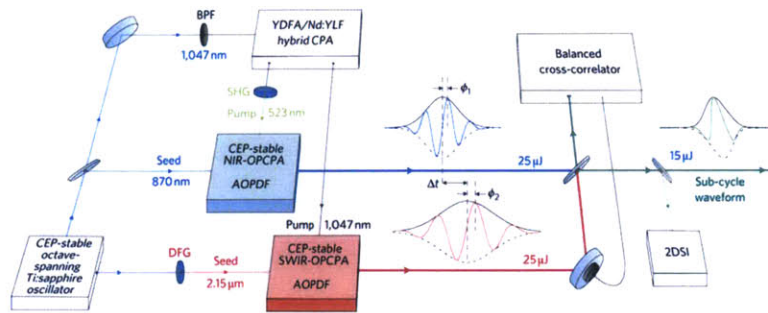
Experiments

3.1 Introduction

The experimental verification of the properties of ADFG requires a fairly sophisticated laser system, which is able to generate a broadband NIR signal with a controllable chirp, optically synchronized with an intense, narrowband, pump, and a variety of pulse characterization instruments to confirm various properties of the system. Furthermore, in order to satisfy the greater goals within the Kaertner group there are additional constraints placed on the system, such as the requirement for CEP stability, constraints on the chirps used in the system, the laser systems used in terms of energy and wavelength, etc. Ultimately, the experimental apparatus described here was created to satisfy all of these constraints, however it is in no way an 'optimal' system, or the only way to put together such a system. However, it was made with the equipment and knowhow available within the group, and works quite well for its purpose.

3.2 Implementation

The starting point for experiments described herein was one of the pulse synthesizers in the Kaertner group, which was designed to generate extremely broadband ($0.75 - 2.4\mu m$), extremely short (less than one optical cycle), and quite energetic

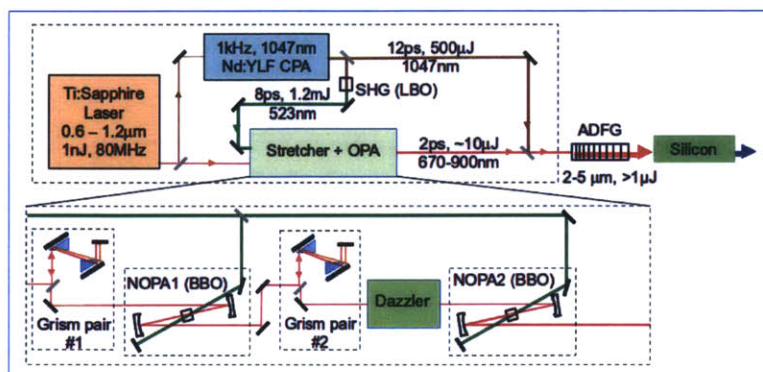


Overview of our pulse synthesizer setup

Figure 3-1: Pulse Synthesizer Overview [13]

(peak powers well in excess of 1GW, with plans to push to nearly 1TW). This system has been published extensively [13] [12] [11] [17] [16] [18], and provides a significant portion of the required laser sources to complete these experiments. A diagram of the system is presented in Figure 3-1, which shows the key components including an octave-spanning Ti:Sapphire oscillator (Menlo Systems Octavius, delivering nJ pulses spanning 590-1170nm), Nd:YLF pump laser system[16] (High-Q and Q-Peak, delivering $3.5mJ$ $12ps$ pulses at 1047nm), and a broadband optical parametric chirped-pulse amplifier (OPCPA) system[12] (delivering $30\mu J$ pulses spanning $0.75 - 1.1\mu m$). Before starting experiments on this project significant improvements were made to the pulse synthesizer, with a focus on improving the long term stability of the system and reducing the amount of labor required to operate the system. This effort included adding an active beam pointing stabilization system to the pump laser, and rebuilding the OPCPA with an improved dispersion management scheme (the prism stretcher was changed to a a prism+grating 'grism' stretcher, to both broaden the bandwidth and improve the pointing stability), more compact layout, and broader bandwidth as needed for seeding this project.

After the initial improvements to the OPCPA system were completed, it was possible to begin the ADFG experiments, which required further modification to the laser system. A complete schematic of the system layout is given in Figure 3-2, which shows that the ADFG experimental setup is quite similar to a normal $800nm$ OPCPA setup. The existing Ti:Sapphire seed and Nd:YLF pump laser were used (unmodified)



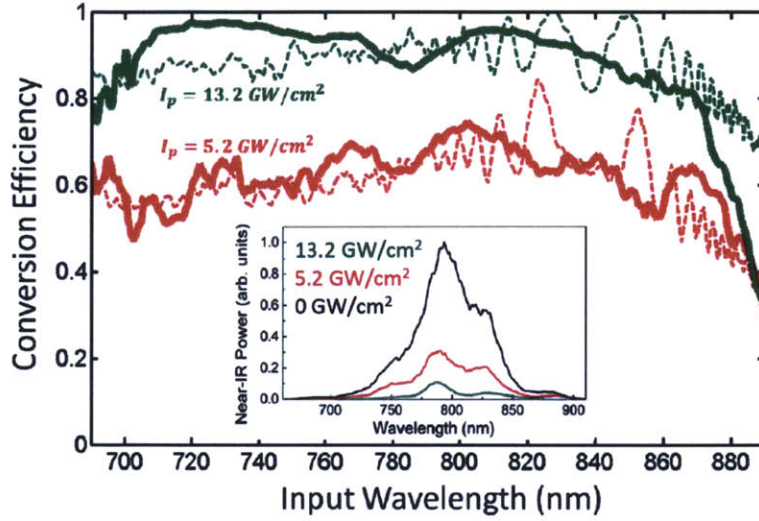
Detail of the ADFG experimental setup

Figure 3-2: ADFG Experimental Setup [25]

to pump a 2-stage OPCPA system (the same system used in the pulse synthesizer), with the existing bulk glass compressor removed and replaced with the combination ADFG crystal (also pumped by the Nd:YLF laser system) and bulk silicon compressor. The ADFG crystal itself consists of a periodically polled magnesium doped lithium niobate crystal (HC Photonics), with a polling period calculated to give good conversion efficiency from $1.2 - 6 \mu\text{m}$ [25]. Polling is a powerful technique in which the direction of the crystal axis is flipped periodically throughout the the crystal, and which allows one to shift the phase matching conditions by adding a 'quasi-phase' [8] to the propagating fields in a well controlled manner.

3.3 Depletion Measurements

The first experiment that attempted to use the ADFG crystal was a depletion measurement, designed to confirm that the ADFG crystal was operating correctly, using the simplest possible experimental setup—to maximize the chances of finding the spatio-temporal overlap. A camera (Dataray WinCam D) was used to spatially overlap the 1047nm pump beam and NIR signal, and a fast photodiode was used to measure the temporal overlap to within a few tens of picoseconds (roughly 1cm of free space propagation). Then a spectrometer (Ocean Optics USB2000) was used to measure the NIR spectrum transmitted through the crystal, with a dichroic mir-



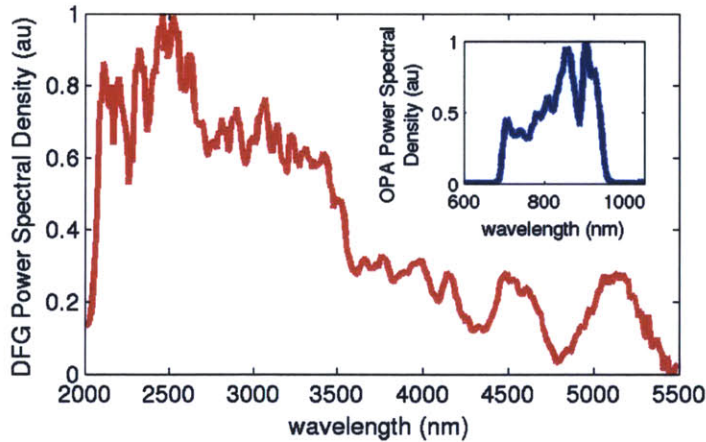
Conversion efficiency, as calculated from the NIR depletion and assuming that all depleted NIR photons are converted to the MIR, plotted against the expected conversion efficiency with a simulated pump intensity approximately 1.6 times higher than the measured pump intensity as the $1.047\mu\text{m}$ pump intensity was increased, and the measured NIR spectra (inset).

Figure 3-3: NIR Depletion [13]

ror used to block the residual 1047nm pump light. The pump intensity was set to $5\text{GW}/\text{cm}^2$ (calculated to give approximately 70% photon conversion), and the temporal overlap between the pump/signal was scanned by means of an optical delay line. As expected, the transmitted NIR signal intensity decreased when the overlap between the pump/signal was found, and a roughly 50% depletion of the pump was observed, (shown in Figure 3-3, red trace) which implies that half of the NIR photons were being converted to the MIR. Furthermore, it was observed that so long as the NIR signal was well centered (temporally and spatially) on the pump the depletion was approximately uniform across the entire 680-880nm bandwidth of seed pulse, which implies that the conversion process was working over the full wavelength range and generating an idler spanning $1.8 - 5.5\mu\text{m}$. The pump intensity was then increased to $13\text{GW}/\text{cm}^2$, to compensate for nonidealities in the crystal, and depletion rose to $> 80\%$, which was an excellent initial confirmation that the ADFG process was working correctly and implied it was generating an idler spanning $1.8 - 5.5\mu\text{m}$, with a $> 80\%$ photon conversion efficiency.

3.4 Generation of Uncompressed Continuum

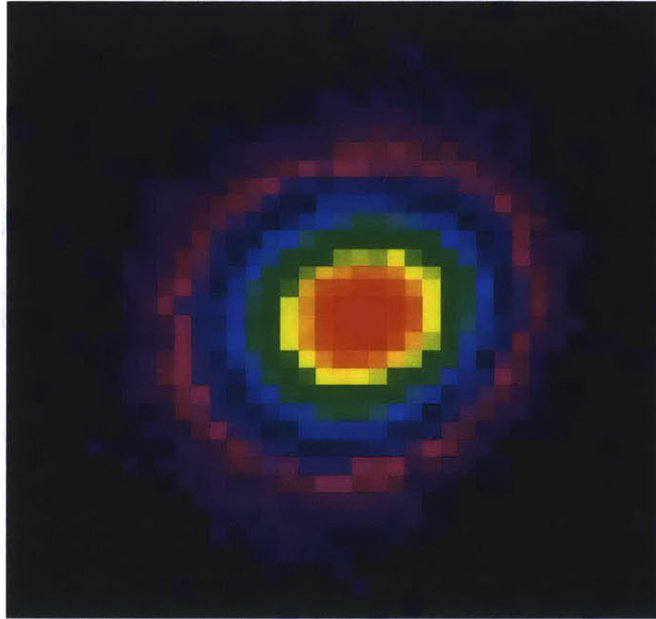
The next logical step was to confirm that the spectrum of the MIR idler matched the simulations. This was slightly complicated by the fact that the MIR idler is generated collinearly with the signal/pump, so it is necessary to use some type of wavelength selective optic to block the signal/pump and pass the idler. Unfortunately, due to the broadband nature of the idler, it is was not practical to use a dichroic mirror (in particular, because the reflected MIR idler also needs to have a clean spectral phase for recompression, which places further constrains on the mirror design), so initial experiments used a piece of bulk silicon which is highly absorbing at the pump wavelength, but quite transparent at the idler wavelength. This worked reasonably well, however it was later discovered that the intense pump (as high as $10\text{GW}/\text{cm}^2$ at the silicon) was causing some absorption of the signal, and it was only possible to get good transmission of the idler if the pump and signal were made slightly non-collinear, such that the idler would be spatially separated from the pump at the silicon block. This situation was not ideal, however a promising alternative was tin-



Measured MIR spectra spanning $2\mu\text{m} - 5.5\mu\text{m}$, generated from the NIR spectra shown in the inset.

Figure 3-4: Uncompressed MIR Spectrum

doped indium oxide (ITO) which is transmissive at wavelengths below the plasma frequency (which occurs at roughly $1.2\mu\text{m}$ in our samples) and reflective at higher



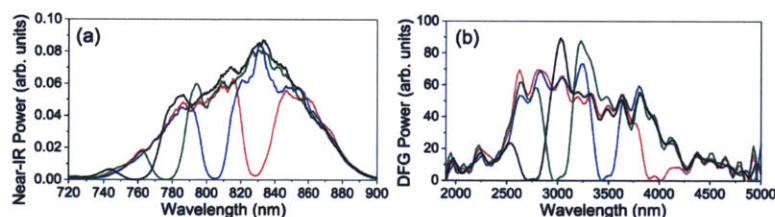
Beam profile of the MIR idler (1 pixel = $100\mu m$)

Figure 3-5: MIR Beam Profile

wavelengths [5], which makes it an ideal candidate to use as a dichroic mirror for this application. This worked well; after 1 bounce off an ITO coated glass substrate the pump intensity was reduced sufficiently as to prevent the absorption in the silicon filter. After we were able to confirm reliable generation of a MIR idler we were able to route the resulting beam into a scanning grating monochromator (Horiba MicroHR), and measure the MIR idler spectra, as shown in Figure 3-4 where we measured a spectrum spanning roughly $2 - 5.5\mu m$. Note the strong absorption at $4.2\mu m$, which is due to absorption of CO_2 in the atmosphere. Furthermore, we used a pyroelectric detector (Molelectron J3-05) to measure the total energy of the MIR idler and found that we were able to generate approximately $1\mu J$ of energy in the idler after the filtering optics. After accounting for the losses in the system (fresnel reflections off the crystal faces, silicon block, leakage through the ITO, quantum defect, etc) we confirmed that there was $> 80\%$ photon conversion to the MIR. Furthermore, we measured the beam profile using a pyroelectric camera (Spiricon, Pyrocam), as shown in Figure 3-5, and confirmed that the beam was clean and round, free of astigmatism or spatial chirp.

3.5 Spectral Amplitude Transfer

After confirming that the MIR idler was being generated as expected, an experiment was conducted to confirm that the amplitude transfer was working as expected—that is to say that the spectral amplitude profile of the NIR seed should be directly transferred to the MIR idler, with a bandwidth determined by the pump, which is approximately $0.2nm$ in this case. We did this by using the acousto-optic programmable dispersive filter (Fastlite, Dazzler) to put a hole in the NIR spectrum, and using the MIR spectrometer to observe the change on the MIR spectrum. As expected, the amplitude profile of the NIR seed was transferred, as shown in Figure 3-6, which shows 4 different NIR input spectra, and the corresponding MIR output spectra, each with a hole on the spectral amplitude profile.

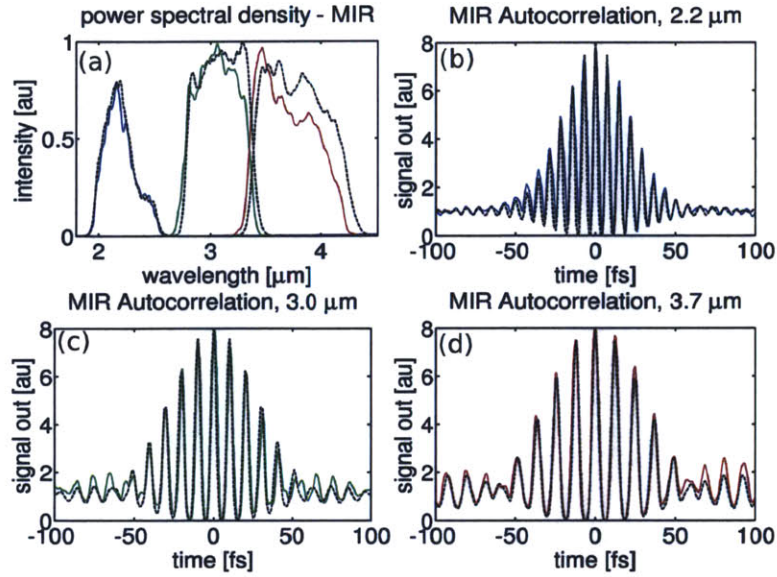


Transfer of the spectral amplitude was confirmed by putting a series of 'holes' in the input spectrum using a Dazzler, plotted in (a), and observed in the MIR spectra (b). Note: the slight peaking effect at the edges of the holes is an artifact from the OPCPA system, and is caused by the fact that there is a highly saturated OPCPA after the dazzler. The amplifier is saturated to the point of back conversion in the $760 - 820nm$ wavelength range, so the reduced seed intensity caused by adding a hole causes the amplified signal to increase slightly at the edges of the hole, as can be seen in the NIR and MIR spectra.

Figure 3-6: Spectral Amplitude Transfer [13]

3.6 Spectral Phase Transfer

The final task to confirm that the ADFG based MIR source was working correctly was to confirm the spectral phase transfer, and the ability to use the spectral phase transfer to transfer a carefully selected chirp on the NIR pulse to the MIR, such as to allow the generated MIR idler to be compressed in a bulk silicon compressor. This was carried out by using a 20mm-long anti-reflection-coated silicon block as the compressor, and using a homemade second-order interferometric autocorrelator (IAC) to generate an interferometric autocorrelation of the pulse, so that the duration could be characterized. Note, an IAC cannot directly retrieve the spectral phase, however by comparing the measured IAC trace with one generated assuming the pulse has been perfectly compressed (flat phase across all wavelengths), one can confirm that the pulse has very little residual spectral phase on it. Another limitation of the IAC is that one needs to find a crystal to generate the second harmonic over the entire bandwidth of the seed pulse. Initially, only a $100\mu\text{m}$ thick BBO (Casix, cut for Type-1 phase matching, $\theta = 24^\circ, \phi = 45^\circ$) and $400\mu\text{m}$ AGS (Eskma, cut for Type-1 phase matching, $\theta = 37^\circ, \phi = 45^\circ$) were available, which limited the bandwidth in the IAC to only support characterization of pulses down to approximately 3 optical cycles. To mitigate this, 3 wavelength bands were selected (one centered at $2.2\mu\text{m}$, which matched well with the BBO crystal, one at $3.0\mu\text{m}$ which works well with the AGS crystal, and one at $3.5\mu\text{m}$, which works with AGS crystal tilted to shift θ such that the phase matching conditions were shifted to longer wavelengths). In each case an extended-InGaAs detector (Thorlabs PDA10DT) was used to detect the generated second harmonic, and an oscilloscope was used to capture the generated interferogram. The results of this experiment is plotted in Figure 3-7, which shows the 4 measured MIR spectra, along with the measured and expected interferograms. The good match between the measured and expected interferograms implies that the generated pulses have a minimal residual phase on them, a confirmation that the spectral phase transfer is working correctly in the ADFG crystal.

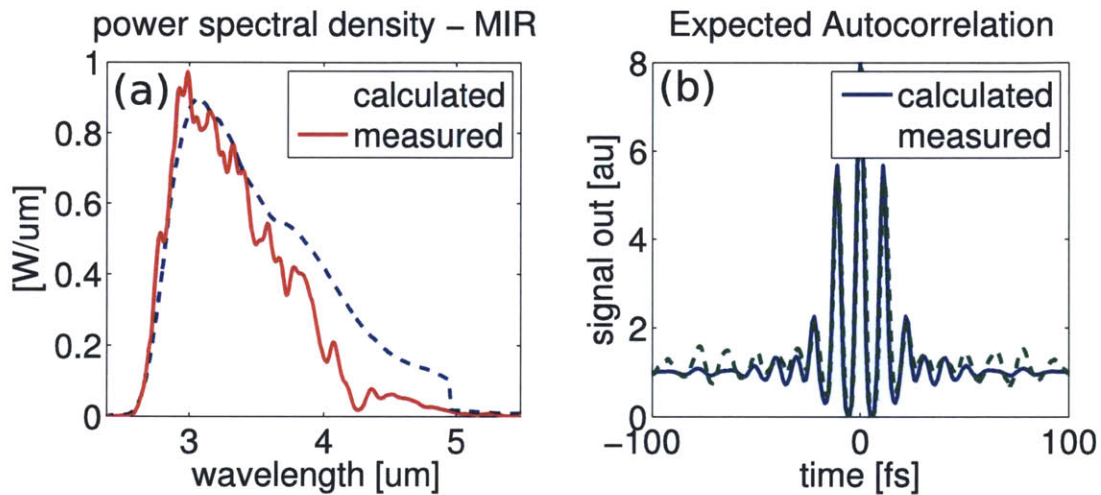


Demonstration of a 4-cycle tunable source, generating a pulse at $2.2\mu\text{m}$ (blue), $3.0\mu\text{m}$ (green), and $3.7\mu\text{m}$ (red), with MIR spectra plotted in (a), along with the expected spectrum for each pulse (black), as calculated from the measured NIR input and assuming 100% photon conversion efficiency to the MIR. Additionally, the 3 measured autocorrelations (b-d), each with an overlay (dashed) calculated as the expected autocorrelation, calculated from the MIR spectrum and assuming perfect (Fourier-limited) compression.

Figure 3-7: 4-cycle Tunable MIR Source

After this initial result, an improved AGS crystal (Eskma, $160\mu\text{m}$ thick $\theta = 37^\circ$, $\phi = 45^\circ$), was purchased and the experiments repeated to confirm that the full bandwidth of the pulse could be compressed simultaneously. This time the limiting factor was the inherent collinear nature of the IAC, which means that one must be able to separate the fundamental signal from the (much weaker) second harmonic by means of a wavelength or polarization selective optic. Due to the limited contrast ratio achievable with MIR polarizers, it was necessary to use spectral filtering to isolate the generated second harmonic, which limited the usable bandwidth of the autocorrelator to one octave. The octave spanning $2.4 - 4.8\mu\text{m}$ was selected for compression, as it worked well with the available filters/detectors, and represents a useful wavelength range for spectroscopic applications. The resulting interferogram is shown in Figure 3-8, which shows the measured MIR spectrum, with the measured and expected IAC trace, as in the tunable 4-cycle source. As with the 4-cycle source,

this result shows it is possible to simultaneously compress the pulse across the full bandwidth ($2.4 - 4.8\mu m$) and generate a pulse with a duration of approximately $20fs$, with a center frequency of $3.6\mu m$, approximately 1.5 optical cycles. Based on the simulation results discussed in Section 2.4 It is expected that by improving the pulse characterization system it should be possible to confirm the generation of a pulse of approximately a single-cycle in duration, and in fact such a pulse may already have been generated by the current system.



Demonstration of a sub-2-cycle source, generating a pulse centered at $3.6\mu m$, with (a) measured MIR spectra and expected MIR spectra calculated from the measured NIR spectra and assuming 100% photon conversion efficiency, and (b) measured autocorrelation, with expected overlay calculated from the measured MIR spectrum and assuming perfect (Fourier-limited) compression

Figure 3-8: Pulse Compressed to Sub-2-Cycle Duration

Chapter 4

Conclusions

Adiabatic difference frequency generation promises the ability to generate extremely broadband MIR laser sources efficiently, with nicely controllable properties—and the applications are not only limited to generating MIR idlers. The process works exactly the same for sum frequency generation [26], and a similar process has been demonstrated by others [22] [15] for increasing the bandwidth of optical parametric amplifiers. This opens up the entire field of chirped pulse amplification to the benefits of adiabatic frequency conversion processes, limited only by the available crystal technologies and funding opportunities. Furthermore, the process is well understood, very robust (insensitive to crystal temperature, fabrication tolerances, beam intensities, etc [27]), and easily adaptable by judiciously choosing a crystal and polling periods. In this work it is demonstrated that it is possible to use ADFG to generate a multi-octave spanning idler ($1.8 - 5.5\mu m$) with controllable spectral phase/amplitude, good beam profile, moderate energy ($1\mu J$) and appreciable peak power (nearly $100MW$), which can be used directly or as a well controlled seed source for further amplification. It is, however, quite the modest result in terms of what is possible using this technology, using less than half of the available bandwidth available in the crystal as designed.

THIS PAGE INTENTIONALLY LEFT BLANK

Bibliography

- [1] Giedrius Andriukaitis, Tadas Balciunas, Skirmantas Alisauskas, Audrius Pugzlys, Andrius Baltuska, Tenio Popmintchev, Ming-Chang Chen, Margaret M. Murnane, and Henry C. Kapteyn. 90 GW peak power few-cycle mid-infrared pulses from an optical parametric amplifier. *Optics Letters*, 36(15):2755–2757, August 2011.
- [2] J. A. Armstrong, N. Bloembergen, J. Ducuing, and P. S. Pershan. Interactions between light waves in a nonlinear dielectric. *Physical Review*, 127(6):1918–1939, September 1962.
- [3] Satoshi Ashihara, Takahiro Mochizuki, Shunsuke Yamamoto, Tsutomu Shimura, and Kazuo Kuroda. Generation of sub 50-fs mid-infrared pulses by optical parametric amplifier based on periodically-poled MgO:LiNbO₃. *Japanese Journal of Applied Physics*, 48(4R):042501, April 2009.
- [4] Robert W. Boyd. *Nonlinear Optics*. Acad. Press, 2 edition, 2003.
- [5] Scott H. Brewer and Stefan Franzen. Indium tin oxide plasma frequency dependence on sheet resistance and surface adlayers determined by reflectance FTIR spectroscopy. *The Journal of Physical Chemistry B*, 106(50):12986–12992, December 2002.
- [6] D. Brida, M. Marangoni, C. Manzoni, S. De Silvestri, and G. Cerullo. Two-optical-cycle pulses in the mid-infrared from an optical parametric amplifier. *Optics Letters*, 33(24):2901–2903, December 2008.
- [7] David Burghoff, Tsung-Yu Kao, Ningren Han, Chun Wang Ivan Chan, Xiaowei Cai, Yang Yang, Darren J. Hayton, Jian-Rong Gao, John L. Reno, and Qing Hu. Terahertz laser frequency combs. *Nature Photonics*, 8(6):462–467, June 2014.
- [8] Mathieu Charbonneau-Lefort, Bedros Afeyan, and M. M. Fejer. Optical parametric amplifiers using chirped quasi-phase-matching gratings i: practical design formulas. *Journal of the Optical Society of America B*, 25(4):463–480, April 2008.
- [9] C. J. Fecko, J. J. Loparo, and A. Tokmakoff. Generation of 45 femtosecond pulses at 3 μm with a KNbO₃ optical parametric amplifier. *Optics Communications*, 241(4-6):521–528, November 2004.

- [10] M. Hemmer, A. Thai, M. Baudisch, H. Ishizuki, T. Taira, and J. Biegert. 18-uJ energy, 160-kHz repetition rate, 250-MW peak power mid-IR OPCPA. *Chinese Optics Letters*, 11(1):013202, January 2013.
- [11] Kyung-Han Hong, Chien-Jen Lai, Jonathas Siqueira, Peter Krogen, Jeffrey Moses, Martin Smrz, Luis E. Zapata, and Franz X. Kärtner. Multi-mJ, kHz, 2.1- μm OPCPA for high-flux soft x-ray high-harmonic radiation. In *Research in Optical Sciences*, OSA Technical Digest (online), page JW2A.5. Optical Society of America, March 2014.
- [12] Shu-Wei Huang, Giovanni Cirimi, Jeffrey Moses, Kyung-Han Hong, Siddharth Bhardwaj, Jonathan R. Birge, Li-Jin Chen, Irina V. Kabakova, Enbang Li, Benjamin J. Eggleton, Giulio Cerullo, and Franz X. Kärtner. Optical waveform synthesizer and its application to high-harmonic generation. *Journal of Physics B: Atomic, Molecular and Optical Physics*, 45(7):074009, April 2012.
- [13] Shu-Wei Huang, Giovanni Cirimi, Jeffrey Moses, Kyung-Han Hong, Siddharth Bhardwaj, Jonathan R. Birge, Li-Jin Chen, Enbang Li, Benjamin J. Eggleton, Giulio Cerullo, and Franz X. Kaertner. High-energy pulse synthesis with sub-cycle waveform control for strong-field physics. *Nat Photon*, 5(8):475–479, August 2011.
- [14] T. H. Maiman. Stimulated optical radiation in ruby. *Nature*, 187(4736):493–494, August 1960.
- [15] B. W. Mayer, C. R. Phillips, L. Gallmann, M. M. Fejer, and U. Keller. Sub-four-cycle laser pulses directly from a high-repetition-rate optical parametric chirped-pulse amplifier at 3.4 μm . *Optics Letters*, 38(21):4265–4268, November 2013.
- [16] J. Moses, S.-W. Huang, K.-H. Hong, O. D. Mucke, E. L. Falcao-Filho, A. Benedick, F. A. Ilday, A. Dergachev, J. A. Bolger, B. J. Eggleton, and F. X. Kaertner. Highly stable ultrabroadband mid-IR optical parametric chirped-pulse amplifier optimized for superfluorescence suppression. *Optics Letters*, 34(11):1639–1641, June 2009.
- [17] Jeffrey Moses and Shu-Wei Huang. Conformal profile theory for performance scaling of ultrabroadband optical parametric chirped pulse amplification. *Journal of the Optical Society of America B*, 28(4):812–831, April 2011.
- [18] Jeffrey Moses, Cristian Manzoni, Shu-Wei Huang, Giulio Cerullo, and Franz X. Kaertner. Temporal optimization of ultrabroadband high-energy OPCPA. *Optics Express*, 17(7):5540–5555, March 2009.
- [19] Jeffrey Moses, Haim Suchowski, and Franz X. Kaertner. Fully efficient adiabatic frequency conversion of broadband ti:sapphire oscillator pulses. *Optics Letters*, 37(9):1589–1591, May 2012.

- [20] Yutaka Nomura, Hideto Shirai, Kenta Ishii, Noriaki Tsurumachi, Alexander A. Voronin, Aleksei M. Zheltikov, and Takao Fuji. Phase-stable sub-cycle mid-infrared conical emission from filamentation in gases. *Optics Express*, 20(22):24741–24747, October 2012.
- [21] Poul B. Petersen and Andrei Tokmakoff. Source for ultrafast continuum infrared and terahertz radiation. *Optics Letters*, 35(12):1962–1964, June 2010.
- [22] C. R. Phillips, B. W. Mayer, L. Gallmann, M. M. Fejer, and U. Keller. Design constraints of optical parametric chirped pulse amplification based on chirped quasi-phase-matching gratings. *Optics Express*, 22(8):9627, April 2014.
- [23] Albert Schliesser, Nathalie Picque, and Theodor W. Hansch. Mid-infrared frequency combs. *Nature Photonics*, 6(7):440–449, July 2012.
- [24] Alexander Sell, Rudiger Scheu, Alfred Leitenstorfer, and Rupert Huber. Field-resolved detection of phase-locked infrared transients from a compact er:fiber system tunable between 55 and 107 THz. *Applied Physics Letters*, 93(25):251107, December 2008.
- [25] Haim Suchowski, Peter R. Krogen, Shu-Wei Huang, Franz X. Kaertner, and Jeffrey Moses. Octave-spanning coherent mid-IR generation via adiabatic difference frequency conversion. *Optics Express*, 21(23):28892–28901, November 2013.
- [26] Haim Suchowski, Dan Oron, Ady Arie, and Yaron Silberberg. Geometrical representation of sum frequency generation and adiabatic frequency conversion. *Physical Review A*, 78(6):063821, December 2008.
- [27] Haim Suchowski, Vaibhav Prabhudesai, Dan Oron, Ady Arie, and Yaron Silberberg. Robust adiabatic sum frequency conversion. *Optics Express*, 17(15):12731–12740, July 2009.
- [28] J. Ward, E. Schlecht, G. Chattopadhyay, A. Maestrini, J. Gill, F. Maiwald, H. Javadi, and I. Mehdi. Capability of THz sources based on schottky diode frequency multiplier chains. In *Microwave Symposium Digest, 2004 IEEE MTT-S International*, volume 3, pages 1587–1590 Vol.3, June 2004.
- [29] Clarence Zener. Non-adiabatic crossing of energy levels. *Proceedings of the Royal Society of London. Series A*, 137(833):696–702, September 1932.